Proteomic analysis of pancreatic cancer stem cells: functional role of fatty acid synthesis and mevalonate pathways

Jessica Brandi [1#], Ilaria Dando [2], Elisa Dalla Pozza [2], Giulia Biondani [2], Rosalind Jenkins [3], Victoria Elliott [4], Kevin Park [3], Giuseppina Fanelli[5], Lello Zolla[5], Eithne Costello [4], Aldo Scarpa [6], Daniela Cecconi [1*] and Marta Palmieri [2]

[1] University of Verona, Department of Biotechnology, Proteomics and Mass Spectrometry Laboratory, Verona, 37134, Italy;

[2] University of Verona, Department of Neuroscience, Biomedicine and Movement, Verona, 37134, Italy;

[3] University of Liverpool, MRC Centre for Drug Safety Science, Department of Molecular & Clinical Pharmacology, Liverpool, L69 3GE, United Kingdom;

[4] NIHR Liverpool Pancreas Biomedical Research Unit, Department of Molecular and Therapeutic Cancer Medicine, Royal Liverpool University Hospital, Liverpool, L69 3GA, United Kingdom;

[5] Department of Ecological and Biological Sciences, University of Tuscia, Viterbo, Italy

[6] University and Hospital Trust of Verona, Applied Research on Cancer Network (ARC-NET) and Department of Pathology and Diagnostics, Verona, 37134, Italy.

* Corresponding author: Daniela Cecconi, PhD,

Mass Spectrometry & Proteomics Lab, Department of Biotechnology, University of Verona, Strada le Grazie 15, 37134 Verona, Italy

Phone: +39 045 8027056; Fax: +39 045 8027929; e-mail: daniela.cecconi@univr.it

ABSTRACT

Recently, we have shown that the secretome of pancreatic cancer stem cells (CSCs) is characterized by proteins that participate in cancer differentiation, invasion, and metastasis. However, the differentially expressed intracellular proteins that lead to the specific characteristics of pancreatic CSCs have not yet been identified, and as a consequence the deranged metabolic pathways are yet to be elucidated.

To identify the modulated proteins of pancreatic CSCs, iTRAQ-based proteomic analysis was performed to compare the proteome of Panc1 CSCs and Panc1 parental cells, identifying 230 modulated proteins. Pathway analysis revealed activation of glycolysis, the pentose phosphate pathway, the pyruvate-malate cycle, and lipid metabolism as well as downregulation of the Krebs cycle, the splicesome and non-homologous end joining. These findings were supported by metabolomics and immunoblotting analysis. It was also found that inhibition of fatty acid synthase by cerulenin and of mevalonate pathways by atorvastatin have a greater anti-proliferative effect on cancer stem cells than parental cells.

Taken together, these results clarify some important aspects of the metabolic network signature of pancreatic cancer stem cells, shedding light on key and novel therapeutic targets and suggesting that fatty acid synthesis and mevalonate pathways play a key role in ensuring their viability.

Introduction

Pancreatic ductal adenocarcinoma (PDAC) is one of the most aggressive solid tumours with a mortality projected to surpass that of breast and colorectal cancer by 2030 in the United States [1]. More than 85% of patients who undergo surgical resection of small pancreatic tumours with clear surgical margins and no evidence of metastasis, die from metastasis within 5 years [2, 3], a finding that is consistent with early spread. Standard chemo- and radiation therapies, as well as new treatments targeting known oncogenes or growth factors, do not offer significant improvement of survival [4]. In line with these clinical observations, in a mouse model of PDAC, cellular dissemination leading to liver metastasis has been demonstrated to occur prior to the formation of an identifiable primary tumour. In addition, these circulating pancreatic cells have been shown to exhibit a mesenchymal phenotype and the expression of typical markers of cancer stem cells (CSCs). The CSC theory of cancer development is now generally accepted to explain the cellular heterogeneity observed within a tumour. Following this paradigm, only small subpopulations of the tumour cells, the CSCs, are capable to self renew, to give rise to a tumour and to recapitulate its heterogeneity by residing at the top of the cellular hierarchy. CSCs potentially explain several phenomena of cancer such as minimal residual disease, resistance to chemo- and radiation therapies, cancer recurrence and metastases [5]. Stem cells from several cancers, both liquid and solid, including PDAC, have been identified and shown to be particularly resistant to a broad spectrum of anticancer drugs [6]. The existence of CSCs has attractive prospective for identification of CSC-targeted therapies through the determination of the crucial molecules regulating the unique CSC properties. However, despite the enormous potential of CSCs as a new diagnostic and therapeutic target for human cancers, the specific molecular features of these cells are still far to be clarified mainly because of the difficulty to isolate sufficient amount of CSCs from tissue samples. Recently, cancer cell lines have been shown to be an alternative source for CSC research. Along these lines, our group has been able to isolate cancer stem-like cells from five out of nine PDAC cell lines [7] and has demonstrated that Panc1 CSCs showed the highest tumoursphere-forming ability and were the most resistant to the action of various anticancer drugs. In order to deepen

the knowledge of the specific molecular features of these cells, a proteomic approach has then been chosen [8]. In particular, the secretome analysis of Panc1 CSCs has identified a total of 43 proteins secreted at higher level by pancreatic CSCs compared to the parental cell line [9]. These data, together with ELISA assays performed on sera of PDAC patients, has suggested that at least one of the highly secreted proteins by CSCs, i.e. ceruloplasmin, is a promising marker for patients negative for CA19-9 [9].

Here, we report the proteomic analysis of the intracellular proteins of Panc1 CSCs and parental cells. We show that in Panc1 CSCs 115 proteins were up-regulated and 115 down-regulated as compared to parental cells. *In silico* functional pathway analysis and network reconstruction based on signalling reactions reported in literature demonstrates a predominant association of the up-regulated proteins with glycolysis/gluconeogenesis, pentose phosphate pathway (PPP), pyruvate-malate cycle, and lipid metabolism and of down-regulated proteins with Krebs cycle, spliceosome and non-homologous end joining. A metabolomic analysis on glycolysis, Krebs cycle and PPP confirmed the modulation of these pathways. Among the identified proteins, fatty acid synthase (FASN) and acetoacetyl-CoA transferase (ACAT2) were among the most highly up-regulated and were chosen for further analysis. Our data indicate that treatment of cells with cerulenin, a specific FASN inhibitor, or with atorvastatin, a specific inhibitor of the 3-hydroxy-3-methyl-glutaryl-coenzyme A reductase (HMGCR), an enzyme located downstream to ACAT2 in the metabolic pathway that produces isoprenoids and cholesterol, preferentially decrease cell viability of Panc1 CSCs compared to parental cells. All our findings constitute a significant advance in the comprehension of PDAC CSC biology and provide interesting potential targets for the therapeutic approaches to PDAC designed to specifically eliminate the CSC cellular component of the tumour.

MATERIALS AND METHODS

Cell culture

The human PDAC cell line Panc1, called here Panc1 parental cells, was grown in RPMI 1640 supplemented with 10% FBS, 2 mM glutamine, and 50 µg/ml gentamicin sulfate (Gibco, Life Technologies). Adherent cells were maintained in standard conditions for a few passages at 37°C with 5% CO_2. Panc1 CSCs were obtained as previously described [7]. Briefly, adherent cells were cultured in CSC medium (i.e. DMEM/F-12, B27, fungizone, penicillin/streptomycin, heparin, epidermal growth factor and fibroblast growth factor) for at least 1-3 weeks or until the appearance of tumourspheres, which were then cultured in CSC medium for at least three passages before initiating the experiments.

Sample preparation

Samples were prepared as previously described [9]. Briefly, Panc1 cells and Panc1 CSCs cell pellet was collected, lysed in 0.5 M TEAB (Sigma) and 0.1% SDS supplemented with protease inhibitor cocktail 1X (Roche), sonicated 3 times for 10 sec, stored at -80°C for 30 minutes and then sonicated again 3 times for 10 sec. Samples were then centrifuged at 14,000 x g for 10 min at 4°C to remove debris, and the supernatants were collected and stored and -80°C. Protein concentration was determined using BCA protein assay (Thermo Scientific).

Protein digestion and iTRAQ labeling

For this experiment, iTRAQ 8-plex reagents (Sciex, Framingham, USA) were used for the simultaneous analysis of the conditioned media [9] and whole cell lysates of Panc1 cells and Panc1 CSCs. The samples labeled with 114, 116, 117, and 121 iTRAQ tags were used for the secretome analysis of and the data have already been published. In the present work were instead analyzed the samples labeled with 113, 115, 117, and 119 tags. In particular, one biological replica of Panc1 cell line and of Panc1 CSC whole cell lysates were labeled with iTRAQ reagent 113 and 115, respectively,

and a second biological replicate (from a different cell culture passage) was labeled in the same order with iTRAQ reagents 117 and 119. Protein digestion, iTRAQ labeling, and peptide fractionation and desalting were carried out as already described [9].

LC-MS/MS analysis and data processing

Desalted fractions were reconstituted in 40 µL 0.1% formic acid and 5 µL aliquots were delivered into a Triple TOF 5600 (Sciex) via an Eksigent NanoUltra cHiPLC System (Sciex) mounted with a microfluidic trap (200 µm x 500 µm ChromXP C18-CL 3 µm 300 Å) and analytical column (15 cm × 75 µm) packed with ChromXP C_{18}−CL 3 µm. A NanoSpray III source was fitted with a 10 µm inner diameter SilicaTip emitter (New Objective, Woburn, USA). The trap column was washed with 2% ACN/0.1% formic acid for 10 min at 2 µL/min. A gradient of 2−50% ACN/0.1% formic acid (v/v) over 90 min was applied at a flow rate of 300 nL/min. Spectra were acquired automatically in positive ion mode using information-dependent acquisition powered by Analyst TF 1.5.1 software (Sciex). Up to 25 MS/MS spectra were acquired per cycle (approximately 10 Hz) using a threshold of 100 counts per s and with dynamic exclusion for 12 s. The rolling collision energy was increased automatically by selecting the iTRAQ check box in Analyst, and manually by increasing the collision energy intercepts by 5. TOF-MS spectra were acquired for 250 ms (mass range 400−1650 Da) and MS/MS spectra for 100 ms each (mass range 100−1400 Da). Mass spectrometer recalibration was performed at the start of every fifth sample using a β-galactosidase digest standard.

Data analysis was performed using ProteinPilot software (Version 4.2, revision 1340, Sciex) using default settings and with bias and background correction applied. The data were searched against UniProt/SwissProt database (2013_2, total 30,309,316 entries, 40,464 human entries searched) using the Paragon algorithm (4.2.0.0, version 1304, Sciex). The mass tolerance for both precursor and fragment ions was 10ppm [10]. The variable modifications selected for the search were 'biological modifications' (probability-based modification search of 461 biological, chemical and artefactual modifications), while the fixed modifications were carbamidomethylation of cysteines, and iTRAQ

modification of C-terminal lysine residues and peptide N-termini. A global FDR value of 1% was used based on the number of proteins identified before 1% of the identifications were derived from a match to the reverse database [11] (equating to an unused score of 1.09 and a confidence of 91.9%). Similarly, a global FDR cut-off of 1% was used as the criterion for acceptance of individual MS/MS spectra and in this case corresponded to a confidence of 93.8%.

Ratios were calculated from the areas under the curve for each iTRAQ reporter ion selecting different denominators depending on the comparisons to be made. Mean ratios were calculated based on all occurrences (up to 7) of all peptides for which there was a peptide confidence of >15% and where the protein was confidently identified through other evidence. Where a single peptide was used for quantification, the peptide confidence cut-off was 95%. Where a single peptide was used for identification, the cut-off was 99%. The Paragon algorithm performs a Student t-test on the unweighted log ratios (for background corrected data) and reports the p-value: for a final error rate of 5% and with 1157 proteins quantified, the Bonferroni correction suggests a significant p-value at 0.0043.

Bioinformatics analysis of identified proteins

Known and predicted protein associations were analyzed and visualized with STRING version 10 software (http://stringdb.org/). We retrieved interactions that were of at least high confidence (score 0.7), based exclusively on experimental and database knowledge, while excluding all other prediction methods implemented in STRING (such as text-mining and co-expression). Additional white nodes and network depth were kept to the minimum value (1), in order to exclude as many false positive interactions as possible.

Moreover, Ingenuity Pathway Analysis (IPA, Ingenuity Systems, Redwood City, CA) was used to perform a comprehensive analysis of modulated proteins that characterized Panc1 CSCs. The IPA Core Analysis allowed to identifying the most significant networks, biological functions, perturbed canonical pathways as well as potential upstream regulators associated with this signature. The settings

were as follows: i) Reference set: Ingenuity Knowledge Base; ii) Relationship to include: Direct and Indirect; iii) Filter Summary: Consider only molecules and/or relationships where (species = Human) AND (confidence = Experimentally Observed).

The most important networks were calculated on the basis of the IPA score (>40) which take into account the number of focus proteins and the size of the network to approximate the relevance of the network to the original list of proteins. Proteins associated with canonical pathways were estimated as significant using Fisher's exact test (p-value ≤ 0.01) to determine the probability that the association between identified proteins and a canonical pathway could be explained by chance alone.

We also performed the IPA Upstream Regulator analysis to identify a putative cascade of upstream transcriptional regulators that can further explain the observed expression changes in Panc1 CSCs. The upstream regulators were assumed as valid effectors of gene/protein expression if the corresponding p-value obtained by Fisher's exact test was ≤ 0.01. Activation z-score algorithm was used to allow for prediction whether an upstream regulator is activated ($z \geq 2$) or inactivated ($z \leq -2$) based on the direction of expressional change of the associated genes.

Western Blot analysis

Western Blot analysis was performed on two independent biological replicates of Panc1 and Panc1 CSCs to validate quantitative data obtained by MS, and on a biological replicate of Panc1 CSCs to verify the level of expression of FASN and of ACAT2 after inhibition of fatty acid synthesis and mevalonate pathways.

Protein samples were diluted 1:1 with Laemmli's sample buffer (62.5 mM Tris-HCl, pH 6.8, 25% glycerol, 2% SDS, 0.01% Bromophenol Blue), heated for 5 min at 95°C and separated by SDS/polyacrylamide gel electrophoresis (PAGE) on 12% T acrylamide gels in Tris/glycine/SDS buffer. Proteins were then electroblotted onto polyvinilydene fluoride membranes (Bio-Rad, Hercules, CA) at 80 V for 1h and 30 min at 4°C. Amido Black staining was used to confirm equal protein loading in different lanes. Non-specific sites were blocked by incubating the membranes with 5% non-

fat dried milk and 0.05% Tween-20 (Sigma-Adrich) in Tris-buffered saline for 1h at room temperature. Membranes were incubated with the primary antibodies at the appropriate dilutions in 1% non-fat dried milk, 0.05% Tween-20 in Tris-buffered saline for 3 h at room temperature. Blots were then incubated 1h at room temperature with the appropriate horseradish peroxidase (HRP)-conjugated secondary antibody (see the **Supplemental Table 1**). The immunocomplexes were visualized by chemiluminescence using the Chemidoc MP imaging system (Bio-Rad Laboratories) and the intensity of the chemiluminescence response was measured by processing the image with Image Lab software (Bio-Rad).

Metabolite extraction

Metabolomic analyses on Panc1 cells and Panc1 CSCs were performed as previously reported [12]. Cells were prepared following the protocol published by Sana et al. [13], with minor modifications as previously reported [12]. The sample was resuspended by adding 0.15 ml of ice-cold ultra-pure water (18MΩ) to lyse cells. The tubes were plunged into dry ice or a circulating bath at -25°C for 0.5 min and then into a water bath at 37°C for 0.5 min. To each tube was added 0.6 ml of -20°C methanol and then 0.45 ml of -20°C chloroform. The tubes were mixed every 5 min for 30 min. Subsequently, 0.15 ml of ice-cold pH-adjusted ultra-pure water was added to each tube and these were centrifuged at 1000xg for 1 min at 4°C, before being transferred to -20°C for 2–8 h. After thawing, liquid phases were recovered and an equivalent volume of acetonitrile was added to precipitate any residual protein. The tubes were then transferred to a refrigerator (4°C) for 20 min, centrifuged at 10,000xg for 10 min at 4°C and the collected supernatants were dried to obtain visible pellets. Finally, the dried samples were re-suspended in 1 ml of water, 5% formic acid and transferred to glass autosampler vials for LC/MS analysis.

Rapid-resolution reverse-phase HPLC for metabolite separation

An Ultimate 3000 Rapid Resolution HPLC system (DIONEX, Sunnyvale, USA) was used to perform metabolite separation. The system featured a binary pump and vacuum degasser, well-plate autosampler with a six-port micro-switching valve, and a thermostated column compartment. A Phenomenex Luna 3µm HILIC 200A (150 × 2.0 mm), protected by a guard column HILIC 4 × 2.0 mm ID (Phenomenex), was used to perform metabolite separation over a phase B to phase A gradient lasting 35 minutes. For the HILIC separation, a solution of 50 mM ammonium acetate was prepared by dissolving ammonium acetate in deionized water. Aqueous ammonium acetate was mixed with acetonitrile (95:5, v/v). This was used for the mobile phase 'A'. The eluent 'B' was composed of a mixture of 50 mM aqueous ammonium acetate: water plus acetonitrile (95:5), v/v). Acetonitrile, formic acid, and HPLC-grade water and metabolite standards (≥ 98% chemical purity) were purchased from Sigma Aldrich.

Mass spectrometry: Q-TOF settings

Due to the use of linear ion counting for direct comparisons against naturally expected isotopic ratios, time-of-flight instruments are most often, being the best choice for molecular formula determination. Thus mass spectrometry analysis was carried out on an electrospray hybrid quadrupole time-of-flight instrument MicroTOF-Q (Bruker-Daltonik, Bremen, Germany) equipped with an ESI-ion source. Mass spectra for metabolite-extracted samples were acquired in negative ion modes. ESI capillary voltage was set at 4500 V (−) ion mode. The liquid nebulizer was set at 27 psi and the nitrogen drying gas was set to a flow rate of 6 L/min. Dry gas temperature was maintained at 200 °C. Data were stored in a centroid mode. Data were acquired with a stored mass range of 50–1200 m/z. Because calibration of the mass analyzer is essential in order to maintain a high level of mass accuracy, instrument calibration was performed externally every day with a sodium formate solution consisting of 10 mM sodium hydroxide in 50% isopropanol: water, 0.1% formic acid. Automated internal mass scale calibration was performed through direct automated injection of the calibration solution at the beginning and at the end of each run by a 6-port divert-valve.

Metabolite data elaboration

Replicates were exported as mzXML files and processed through MAVEN.52; mass spectrometry chromatograms were elaborated for peak alignment, matching and comparison of parent and fragment ions, and tentative metabolite identification (within a 10 ppm mass-deviation range between observed and expected results against the imported KEGG database). MAVEN is an open-source software that could be freely downloaded from the official project websites (http://genomics-pubs.princeton.edu/mzroll/index.php?show=download). Results were graphed with Graphpad Prism 5.01 (Graphpad Software Inc). Statistical analyses were performed with the same software, as a result of paired t-test or two-way ANOVA among the results obtained from Panc1 and Panc1 CSCs.

Cerulenin and atorvastatin treatments, cell proliferation assay and morphologic changes

Cerulenin and atorvastain were obtained from Sigma-Aldrich St. Louis, MO. Cerulenin was dissolved in ethanol at a final concentration of 20 mg/ml and stored at -20°C. Atorvastatin was dissolved in dimethyl sulfoxide (DMSO, Sigma-Aldrich) at a final concentration of 10 mg/ml and stored at room temperature. Panc1 and Panc1 CSCs (5×10^3 cell/well) were cultured in 96-well plates and incubated at 37°C with 5% CO_2. Twenty-four hours later, cells were treated with a serial concentration of cerulenin (0, 5, 10, 25, 50, 100, 250, and 500 μM) or of atorvastatin (0, 2.5, 5, 10, 25, 50, 100, and 250 μM). Three independent experiments were performed.

After 48 h of each treatment, resazurin dye solution was added in an amount equal to 10% of the culture medium volume and plates were incubated for 1 h at 37°C with 5% CO_2. Metabolic activity of living cells was measured fluorometrically by monitoring the increase in fluorescence at a wavelength of 590 nm, using an excitation wavelength of 535 nm on an automatic microplate reader. The effect of inhibitors on cellular morphology was assessed by collecting phase-contrast microscopy images of Panc1 and Panc1 CSCs cells after 48 h.

Statistical analysis

The data for inhibitors-treated cells and non-treated controls were compared using two-way analysis of variance (ANOVA) and Student's t-test. P-values less than 0.05 were regarded statistically significant. All data were processed using GraphPad Prism Software Version 6.0 (La Jolla, CA, USA).

RESULTS

Differential profile of the whole cell proteome in Panc1 CSCs respect to Panc1 cells

Protein expression profiles of Panc1 cells and Panc1 CSCs were investigated using the iTRAQ approach. A total of 2045 proteins with at least 93.8% confidence and an Unused ProteinPilot scores > 1.09 (equating to a global FDR of 1%) were identified and among them 1157 proteins were quantified (**Supplemental Table 2**). Of these, 608 were identified via a single peptide with a confidence of 99% (**Supplemental Table 3**). Differential protein expression was considered to be significant when the expression increased or decreased with a fold change of 1.5 and a p value smaller than 0.05 in both biological replicates. A total of 230 proteins were found differentially expressed (**Supplemental Table 4**) and among them 115 proteins were up-regulated and 115 down-regulated in Panc1 CSCs as compared to Panc1 parental cells.

Interaction networks, pathway analyses, and upstream regulators of Panc1 CSC proteins

STRING analysis emphasized that the majority of the differentially expressed Panc1 CSC proteins interact within established complexes or have functional relationships.

The most striking pathways involving the proteins up-regulated in Panc1 CSCs compared to parental cells belong to carbon metabolism and are, in particular, glycolysis/gluconeogenesis, pyruvate metabolism, biosynthesis of amino acids, and pentose phosphate pathway (**Fig. 1**). On the contrary, the down-regulated proteins are mainly involved in the interactions with molecular components of the spliceosome and non-homologous end joining (**Fig. 2**).

To reveal significant networks and biological functions relevant to Panc1 CSCs, we also performed an IPA. The up-regulated proteins show the highest-score for networks including cell death and survival, cellular assembly and organization, cell-to-cell signalling and interaction, cellular development, growth and proliferation, and carbohydrate metabolism, while the down-regulated proteins are involved in cell death and survival, cellular growth and proliferation, and RNA post-transcriptional modification (**Supplemental Fig 1**)**.** Next, we systematically evaluated the biological functions of the identified proteins. Most of the regulated Panc1 CSC proteins appear to be involved in cancer, cellular growth and proliferation (**Table 1**). In particular, the up-regulated proteins are specifically involved in cellular movement and free radical scavenging, while the down-regulated proteins are specifically connected to the post-transcriptional modification of RNA and to cellular response to therapeutics. Overall, IPA software revealed that the Panc1 CSC modulated proteins show a significant link with 21 or 19 different pathways for up- or down-regulated proteins, respectively (**Supplemental Table 5**). The ten top canonical pathways (p-value ≤ 0.001) are shown in **Figure 3**. Among the most statistically significant canonical pathways, glycolysis (P-value: 7.94 E-11) and gluconeogenesis (P-value: 1.12 E-10) are included for the up-regulated proteins and DNA double-strand break repair by non-homologous end joining (P-value: 1.23 E-06) and telomere extension by telomerase (P-value: 1.66 E-06) for the down-regulated proteins.

Finally, the IPA software allowed us to examine also the potential upstream regulators associated with the above-described proteomic profiles. In particular, the upstream regulators predicted to be significantly activated include the transcription factors HIF1A (p = 1.29E-09, z = 2.228) and SMARCA4 (p = 5.36E-06, z = 2.219), as well as the estrogen-related receptor gamma ESRRG (p = 4.24E-07, z = 2.180), while the transcription factor NR1H4 (p = 2.08E-05, z = -2.236) is predicted to be inhibited in Panc1 CSCs. A complete list of transcriptional upstream regulators with significant p-values ($p \leq 0.01$) can be found in **Supplemental Table 6**.

Western blot analyses of selected proteins identified by iTRAQ

Seventeen differentially expressed proteins (ten up-regulated and seven down-regulated in Panc1 CSCs), for which commercial antibodies were available, were selected for validation using Western blot analyses. The expression level of proteins in Panc1 cells and Panc1 CSCs were compared on two biological replicates. As shown in **Figure 4,** Western blot results are consistent with the MS quantification data. Notably, in Panc1 CSCs relative to parental cells, MARCKS is up-regulated at intracellular level only as intact (~ 80 kDa), but not as cleaved (~ 40 kDa) form and more isoforms of Integrin beta-1 (ITGB1) and hnRNP A2/B1 (HNRNPA2B1) are immunodetected and all appear to be down-regulated.

Metabolomic analysis of Panc1 CSCs

Since the proteomic analysis revealed that carbon metabolism (mainly glycolysis and pyruvate metabolism) is the pathway that characterizes the proteins induced in Panc1 CSCs (**Fig. 1**), we determined fold-change variations of the concentration levels of several key metabolites of glycolysis, Krebs cycle, and the energetic metabolism. **Figure 5A** shows that the glycolytic intermediates are mainly present at higher level in Panc1 CSCs in comparison to Panc1 parental cells. In particular, Panc1 CSCs show a significant increase in glucose-6 phosphate, fructose-1,6 bisphosphate, glyceraldehyde-3 phosphate, and lactate, while pyruvate decreases. We next investigated whether the accumulation of glycolytic intermediates was associated to an increase in refueling of pentose phosphate pathway (PPP). Interestingly, Panc1 CSCs reveal the accumulation of PPP intermediates, both of the oxidative phase (D-gluconic acid and D-ribose 5-phosphate) and non-oxidative phase (sedoheptulose 7-phosphate and D-xylulose phosphate) (**Figure 5B**). In line with the increased level of glycolysis metabolites, Krebs cycle intermediates including succinate, fumarate, and malate are decreased and two Krebs cycle-related metabolites, glutamine and glutamate, are decreased and increased, respectively, in Panc1 CSCs compared to Panc1 P cells (**Figure 5C**).

Decreased cell viability of Panc1 CSCs in response to inhibition of fatty acid synthesis and mevalonate pathways

The observation that FASN was expressed at 18 fold higher level in Panc1 CSCs compared to Panc1 cells led us to investigate the role of fatty acid synthesis in Panc1 CSC viability. For this purpose, we tested the effect of cerulenin, a specific FASN inhibitor, on the proliferative activity of Panc1 cells and Panc1 CSCs. The cell viability assay was performed 24 (data not shown) or 48 hours after the beginning of the treatment with cerulenin at concentrations ranging from 0 to 500 μM. As shown in **Figure 6A,** cerulenin is able to decrease cell viability at a significantly higher level in Panc1 CSCs compared to Panc1 cells with IC_{50} values of 15.6 μM ± 1.3 and 24.2 μM ± 1.7, respectively. This result strongly suggests an increased cell viability role of fatty acid synthesis in CSCs compared to parental cells.

In a parallel experiment, conceived on the observation that ACAT2 was expressed at 21 fold higher level in Panc1 CSCs compared to Panc1 cells, we examined the role of isoprenoids/cholesterol synthesis in Panc1 CSC viability. For this purpose, we used the drug atorvastatin, which is known to specifically inhibit HMG-CoA reductase, an enzyme located downstream to ACAT2 in the metabolic pathway that produces isoprenoids and cholesterol. We cultured both Panc1 cells and Panc1 CSCs for 24 (data not shown) and for 48 hour with atorvastatin at concentrations ranging from 0 to 250 μM. As shown in **Figure 6B,** atorvastatin strongly inhibits the viability of Panc1 CSCs, while only slightly reduces that of Panc1 cells, with IC_{50} values of 43 μM ± 24.8 and > 250 μM, respectively. This result strongly suggests an increased cell viability role of isoprenoids/cholesterol synthesis in CSCs compared to parental cells.

To verify whether treatments with cerulenin and atorvastatin had an effect on the expression level of FASN and ACAT2 and to ascertain that the up-regulation of FASN observed in Panc1 CSCs was not a consequence of the presence of growth factors in the culture medium [14], a western blot analysis was performed. As shown in **Figure 7,** FASN level is independent of the presence of EGF and FGF in the culture medium and is not modulated by the treatment with the specific inhibitor cerulenin,

which is a covalent inactivator of the β-ketoacyl synthase reaction on FAS. On the contrary, the expression level of ACAT2 in Panc1 CSCs appears to be increased after the inhibition of the mevalonate pathway by atorvastatin.

Morphologic changes of Panc1 cells and Panc1 CSCs in response to the inhibition of fatty acid synthesis and mevalonate pathways

To evaluate if the inhibition of fatty acid synthesis had an effect on cellular morphology, we examined cells by a phase-contrast microscope at 48 hours after treatment with 0, 25, 100 or 250 μM cerulenin. Before treatment, Panc1 cells exhibited a typical epithelial morphology with intact cell-to-cell contacts, while Panc1 CSCs exhibited a mesenchymal morphology with cell aggregates (or spheroids) and a more dispersed colony appearance suggesting an epithelial mesenchymal transition (EMT) phenotype. Interestingly, after cerulenin treatment, Panc1 cells exhibited only a decreased cell-to-cell contact, while Panc1 CSCs showed drastic changes in cell morphology, with reduction of spheroids suggesting cytoskeletal reorganization (**Fig. 8A**). The analysis also indicated that the anti-proliferative/viability effect was due, at least in part, to the decrease in cell number after cerulenin treatment.

We also evaluated the effect of atorvastatin on the morphology of Panc1 cells and Panc1 CSCs. As shown in **Figure 8B,** the effect on cell morphology of this inhibitor was similar to that of cerulenin. Phase-contrast microscopy images show in fact that after atorvastatin treatment Panc1 CSCs were characterized by a reduction of spheroids suggesting cytoskeletal reorganization, while Panc1 cells exhibited a decrease in cell-to-cell contacts. In addition, Panc1 CSCs were rounded and detached after atorvastatin treatment.

DISCUSSION

Activated metabolic pathways in Panc1 CSCs

Our previous study [9] showed higher secretion level of different proteins in Panc1 CSCs compared with the parental cells, and hence suggested possible involvement of these proteins in the processes of pancreatic cancer differentiation, invasion, and metastasis.

In the present study, with the aim of further deepening the understanding of pancreatic CSC biology, we carried out a proteomic analysis of Panc1 and Panc1 CSC whole-cell extracts to investigate the intracellular molecular mechanisms characterizing pancreatic CSCs. The data obtained revealed the regulation of some key metabolic pathways in Panc1 CSCs (**Fig. 9**).

Our proteomic results indicate that glycolysis and gluconeogenesis (**Fig.1** and **Fig. 3**), previously reported to be involved in the secretome of both Panc1 cells and Panc1 CSCs [9], are also strongly represented by intracellular up-regulated proteins in Panc1 CSCs. In particular, data show that fructose-bisphosphate aldolase A (ALDOA, +15.31), triosephosphate isomerase (TPI1, +13.25), glyceraldehyde-3-phosphate dehydrogenase (GAPDH, +9.21), phosphoglycerate kinase 1 (PGK1, +2.37), phosphoglucomutase-1 (PGM1, +18.29), phosphoglycerate mutase 1 (PGAM1, +12.26), alpha-enolase (ENOA, +13.48), and pyruvate kinase isozymes M1/M2 (PKM, +18.76) are all more highly expressed in Panc1 CSCs than in the parental cells. Furthermore, Panc1 CSCs also express an increased level of both L-lactate dehydrogenase A and B chains (LDHA +10.12, LDHB +15.13), which indicates an accentuation of the Warburg effect. According to these data, the upstream regulator analysis performed *in silico* by IPA has identified, among other activated regulators, the transcription factor HIF1A. Indeed, HIF1α, which is typically up-regulated even in solid malignancies in normoxia, modulates stem cell fate reprogramming through glycolytic shift and upregulation of PKM2 [15, 16]. Notably, it has also been demonstrated that HIF1A promotes pancreatic ductal adenocarcinoma invasion and metastasis by activating transcription of the actin-bundling protein fascin [17]. In line with this finding, we found that fascin is up-regulated 7.06 fold in Panc1 CSCs as compared to parental cell line (see **Suppl. Table 4**).

In agreement with the increased expression of glycolytic enzymes, our metabolomic data show that in CSCs the level of glucose-6 phosphate is enhanced, suggesting an increased activity of exokinase in CSCs, despite its expression not differing between cell lines, as shown by the proteomic data. The other glycolytic intermediates that were analysed were present at higher levels in CSC compared to parental cells, though the 2-phopshoglycerate level was not significantly different, confirming a more glycolytic metabolism for CSCs. In line with this observation and with the proteomic data, the level of lactate is also significantly higher in CSCs than in parental cells.

The recent literature describes CSCs as being primarily glycolytic or preferentially relying on oxidative phosphorylation depending on tumour-type and microenvironment [18]. However, it has been shown that in glucose rich environments, proliferating CSCs primarily utilize aerobic glycolysis for their bioenergetic needs, while in glucose (and oxygen) deprived conditions, CSCs shift to a quiescent, slow cycling state relying on mitochondrial oxidative metabolism [19]. In particular, the activation of the glycolytic programme favours stemness via various mechanisms [20, 21], including enhanced antioxidative capacity, with pentose phosphate pathway (PPP) being the most relevant. Our results indicate that several up-regulated proteins of Panc1 CSCs belong to "free radical scavenging" among top biological functions (**Table 1**) and to PPP as a statically significant perturbed pathway (**Fig. 1** and **Fig. 3**). Among PPP enzymes, Panc1 CSCs show over-expression of glucose-6-phosphate 1-dehydrogenase (G6PD, +5.61), 6-phosphogluconate dehydrogenase (PGD, +11.67), and transketolase (TKT, +5.66). These results are also confirmed by the metabolomic analysis which highlights the increase of PPP intermediates (**Fig. 9)**. The PPP is a major glucose metabolic pathway required for cellular demands of anabolism and antioxidant defence. Indeed, the main purpose of PPP is to regenerate NADPH from NADP+ through an oxidation/reduction reaction. This reaction is coupled to the formation of ribose 5-phosphate from glucose 6-phosphate, thus making PPP among the major metabolic pathways involved in malignancies [22]. Our data show increase of metabolic intermediates and byproducts especially of the oxidative phase of PPP (D-gluconic acid and D-ribose 5-phosphate). The increase of oxidative phase intermediates might be explained through diversion to purine salvage

pathway (PSP), as observed in red blood cell [23]. Purine nucleotides may be synthesized in cells *de novo* or reconstructed from already existing free purine bases through the salvage reactions (reutilization) [23].

In Panc1 CSCs, in line with the up-regulation of enzymes involved in glycolysis and PPP, we also observed an induction of enzymes involved in the pyruvate-malate cycle (citrate-pyruvate cycle) (**Fig.1** and **Fig. 3**), i.e. the cytosolic ATP-citrate synthase (ACLY, +2.77), cytoplasmic malate dehydrogenase (MDH1, +10.17) and cytosolic NADP-dependent malic enzyme (ME1, +12.19). This pathway is responsible for citrate transport out of the mitochondria into the cytosol where it is cleaved by ACLY to oxaloacetate and acetyl-CoA, which is available for fatty acid synthesis. On the other hand, cytosolic oxaloacetate is hydrogenated by MDH1 to give NAD^+ and malate, which is then oxidized by ME1 to pyruvate in a reaction which also provides NADPH mainly for fatty acid synthesis. Thus, NADH generated in glycolysis is converted to NADPH for fatty acids synthesis, while simultaneously regenerating the NAD^+ needed to continue glycolysis [24]. Recently, it has been reported that PDAC cells rely on the pyruvate-malate cycle to increase the NADPH/NADP (+) ratio, and that oxaloacetate is produced by a metabolic reprogramming mediated by the KRAS oncogene [25]. Accordingly, we demonstrate that Panc1 cells, which are known to possess a KRAS mutation [26], express enzymes of the pyruvate-malate cycle and that these enzymes are even more expressed in Panc1 CSCs.

Consistently with the up-regulation of enzymes involved in glycolysis, PPP, and pyruvate-malate cycle, we also found that Panc1 CSCs have a strong induction of two cytosolic enzymes involved in lipid metabolism, the cytosolic acetylCoA acetyl transferase (ACAT2, +21.19 fold), which synthesize acetoacetylCoA in the mevalonate pathway leading to cholesterol, and the fatty acid synthase (FASN, +18.36 fold), which synthesize fatty acids.

Recently, in proliferating cells, it has been demonstrated that NADPH production, beyond the important contribution of PPP and the malic enzyme (ME1), originates from the serine-driven one-carbon metabolism, in which oxidation of methylene tetrahydrofolate to 10-formyl-tetrahydrofolate is

480 catalysed by the methylene tetrahydrofolate dehydrogenase (MTHFD) with the reduction of NADP to
481 NADPH [27]. Our data demonstrate for the first time that Panc1 CSCs are characterized by increased
482 levels of the cytosolic MTHFD1 (+3.19) compared to parental cells suggesting that stemness requires a
483 higher contribution of the folate pathway for NADPH homeostasis.
484
485 **Repressed pathways in Panc1 CSCs**
486 As a further confirmation of a switch to a glycolytic metabolism at the expense of the
487 mitochondrial oxidative metabolism, Panc1 CSCs also show a down-regulation of some key enzymes
488 of the Krebs cycle (**Supplemental Table 4**). In support of these results, the metabolomic data show
489 that the level of three Krebs cycle intermediates, i.e. succinate, fumarate, and malate, is significantly
490 decreased in CSCs in comparison to parental cells (**Fig. 5B**). Furthermore, glutamine level is decreased
491 in CSCs compared to P cells, suggesting either a less active glutamine-transport inside the cell or a
492 greater conversion of glutamine to glutamate. Indeed, glutamate level is enhanced in CSCs compared
493 to parental cells, suggesting a minor incorporation of glutamate in the mitochondrion and, together
494 with the other results, a less active Krebs cycle in CSCs in comparison to parental cells.
495 In Panc1 CSCs, proteins involved in spliceosome formation and non-homologous end joining
496 pathway appear to be down-regulated compared to Panc1 cells (**Fig.2** and **Fig.3**), in particular, several
497 hnRNPs (A1, A3, A/B, A2/B1, C1/C2, H3, K, L, M, U, Q), two splicing factors (3B subunit 2, 1
498 serine/arginine-rich), and the RNA-binding protein 25. The down-regulation of multiple types of
499 hnRNPs may represent a strategy of stem cells to keep their undifferentiated state. Indeed, it has been
500 demonstrated that hnRNPs play a key role in the stem cell differentiation process, as for example in the
501 case of embryonic stem cells differentiated into smooth muscle cell, or of multipotent hematopoietic
502 stem cells differentiated into the different types of blood cell, or of neural stem cell differentiated into
503 neuronal cells [28].
504 The non-homologous end-joining (NHEJ) pathway is one of the main mechanisms for repairing
505 breaks in double-stranded DNA. In Panc1 CSCs, representative proteins of this pathway (**Fig.2** and

Fig.3), i.e. poly [ADP-ribose] polymerase 1 (PARP1, -1.96), DNA-dependent protein kinase catalytic subunit (PRKDC, -2.27), and X-ray repair cross-complementing proteins 5 and 6 (XRCC5 -1.89, XRCC6 -1.92), are down-regulated. Interestingly, PARP1 is a pro-apoptotic enzyme [29], the expression of which has been shown to be specifically reduced in stem cells with spherical morphology as compared to monolayer cells [30]. Furthermore, XRCC5 and XRCC6 encode for Ku80 and Ku70 proteins, which form the Ku heterodimer that is involved in repairing double-strand breaks in DNA for maintaining the integrity of genome function. Either Ku70 or Ku80 themselves have also unique functions that are independent of the other Ku subunit [31], as for instance the tumour suppressor activity of Ku70 [32]. In particular, it has been reported that colonic epithelial cells of mice with Ku70 deficiency and $p53^{R172P}$ mutation ($Ku70^{-/-}PP$) show higher rates of proliferation and induction of β-catenin/Wnt pathway, which is important in promoting EMT. Notably, our previous data demonstrated that Panc1 CSCs express higher levels of typical EMT markers compared to parental cells [7].

Functional role of fatty acid synthesis and mevalonate pathways in Panc1 CSC viability

Among the most strongly induced proteins of Panc1 CSCs, we found of particular interest FASN and ACAT2 that, as mentioned above, are involved in lipid metabolic pathways. Notably, high expression level of FASN has been linked to a significantly poor prognosis of PDAC patients and it has been shown to depend upon the induction of EGFR/ERK signalling [14]. Furthermore, FASN has been shown to promote EMT in many cancers, including ovarian [33], breast [34] and colorectal [35] cancer. Our results demonstrate that the overexpression of FASN in Panc1 CSCs is independent of the presence of EGF and FGF in the medium, suggesting a constitutive activation of the EGFR/ERK pathway.

Inhibition of FASN is known to selectively target cancer cells for apoptosis, mainly by interfering with membrane function, inhibiting DNA replication and anti-apoptotic proteins, and accumulating the malonyl-Co-A substrate [36]. Cerulenin is a natural FASN inhibitor that binds

specifically and irreversibly to the β-ketoacyl synthase domain of FASN, thus preventing the condensation reaction between the elongating fatty acid and successive malonyl residues. Interestingly, our results show that cerulenin inhibits Panc1 and Panc1 CSC proliferation, with a greater anticancer activity on stem cells (**Fig.6A**). This is a new observation that could open novel lines of investigation for the development of PDAC CSC target specific therapeutic strategies.

The other metabolic pathway that caught our attention was the mevalonate pathway, which is involved in cholesterol production, because of the strong up-regulation in Panc1 CSCs of ACAT2, one of its key enzymes. The mevalonate pathway affects cancer metastasis in several ways by influencing EMT, cytoskeleton remodelling, as well as cell motility and polarity (non-canonical Wnt/planar pathway). Statins are competitive inhibitors of this pathway by acting on the enzyme the 3-hydroxy-3-methyl-glutaryl-coenzyme A reductase (HMGCR) and blocking the conversion of HMG-CoA to mevalonate. The statins occupy the catalytic site of HMGCR at the level of the binding site for HMG-CoA, thus blocking the access of this substrate to the active site. In the last two decades, the successful and widespread uses of statin drugs for hypercholesterolaemia have revealed their potential anticancer effects demonstrating that the use of statins is associated with reduced cancer-related mortality [37]. Inhibition of mevalonate pathway by statins has shown to have an antitumour effect against certain CSCs, but their effects have never been investigated on pancreatic CSCs [38]. Our data demonstrate that atorvastatin, a synthetic statin, inhibits cell growth of both Panc1 cells and Panc1 CSCs and that CSCs are considerably more sensitive than parental cells (**Fig.6B**), suggesting ACAT2 as a potential target for PDAC CSC specific therapy. In conclusion, the different cytotoxic effects by inhibiting fatty acid synthesis and mevalonate pathways on Panc1 and Panc1 CSCs suggest that the acute reduction of fatty acids or cholesterol production *per se* are not the major source of cell injury, but could target specific stemness characteristics.

In summary, the proteomic and metabolomic analysis on Panc1 cells and Panc1 CSCs highlighted the main metabolic routes used by pancreatic cancer stem cells to survive, proliferate and disseminate in distinct healthy tissues. In particular, these data indicate that the maintenance of high

fatty acid synthesis and mevalonate pathway levels could make critical contribution to survival of pancreatic cancer stem cells. Although targeting tumour metabolism is still in the early days of translation to patients, the improvement on knowledge of deranged metabolic pathways, in particular in cancer stem cells, will accelerate the development of novel therapeutic strategies.

REFERENCES

[1] Rahib L, Smith BD, Aizenberg R, Rosenzweig AB, Fleshman JM, and Matrisian LM. Projecting cancer incidence and deaths to 2030: the unexpected burden of thyroid, liver, and pancreas cancers in the United States. Cancer Res 2014; 74: 2913-21.

[2] Neoptolemos JP, Stocken DD, Friess H, Bassi C, Dunn JA, Hickey H, et al. A randomized trial of chemoradiotherapy and chemotherapy after resection of pancreatic cancer. N Engl J Med 2004; 350: 1200-10.

[3] Abbruzzese JL, and Hess KR. New option for the initial management of metastatic pancreatic cancer? J Clin Oncol 2014; 32: 2405-7.

[4] Rhim AD, Mirek ET, Aiello NM, Maitra A, Bailey JM, McAllister F, et al. EMT and dissemination precede pancreatic tumor formation. Cell 2012; 148: 349-61.

[5] Islam F, Qiao B, Smith RA, Gopalan V, and Lam AK. Cancer stem cell: fundamental experimental pathological concepts and updates. Exp Mol Pathol 2015; 98: 184-91.

[6] Abdullah LN, and Chow EK. Mechanisms of chemoresistance in cancer stem cells. Clin Transl Med 2013; 2: 3.

[7] Dalla Pozza E, Dando I, Biondani G, Brandi J, Costanzo C, Zoratti E, et al. Pancreatic ductal adenocarcinoma cell lines display a plastic ability to bidirectionally convert into cancer stem cells. Int J Oncol 2015; 46: 1099-108.

[8] Cecconi D, and Zamo A. Proteomics of human cancer tissues and cells. Trac-Trends in Analytical Chemistry 2011; 30: 346-59.

[9] Brandi J, Pozza ED, Dando I, Biondani G, Robotti E, Jenkins R, et al. Secretome protein signature of human pancreatic cancer stem-like cells. J Proteomics 2016; 136: 1-12.

[10] Shilov IV, Seymour SL, Patel AA, Loboda A, Tang WH, Keating SP, et al. The Paragon Algorithm, a next generation search engine that uses sequence temperature values and feature probabilities to identify peptides from tandem mass spectra. Mol Cell Proteomics 2007; 6: 1638-55.

[11] Tang WH, Shilov IV, and Seymour SL. Nonlinear fitting method for determining local false discovery rates from decoy database searches. J Proteome Res 2008; 7: 3661-7.

[12] D'Alessandro A, Gevi F, and Zolla L. A robust high resolution reversed-phase HPLC strategy to investigate various metabolic species in different biological models. Mol Biosyst 2011; 7: 1024-32.

[13] Sana TR, Waddell K, and Fischer SM. A sample extraction and chromatographic strategy for increasing LC/MS detection coverage of the erythrocyte metabolome. J Chromatogr B Analyt Technol Biomed Life Sci 2008; 871: 314-21.

[14] Bian Y, Yu Y, Wang S, and Li L. Up-regulation of fatty acid synthase induced by EGFR/ERK activation promotes tumor growth in pancreatic cancer. Biochem Biophys Res Commun 2015; 463: 612-7.

[15] Prigione A, Rohwer N, Hoffmann S, Mlody B, Drews K, Bukowiecki R, et al. HIF1alpha modulates cell fate reprogramming through early glycolytic shift and upregulation of PDK1-3 and PKM2. Stem Cells 2014; 32: 364-76.

[16] Cheng Y, Chen G, Hong L, Zhou L, Hu M, Li B, et al. How does hypoxia inducible factor-1alpha participate in enhancing the glycolysis activity in cervical cancer? Ann Diagn Pathol 2013; 17: 305-11.

[17] Zhao X, Gao S, Ren H, Sun W, Zhang H, Sun J, et al. Hypoxia-inducible factor-1 promotes pancreatic ductal adenocarcinoma invasion and metastasis by activating transcription of the actin-bundling protein fascin. Cancer Res 2014; 74: 2455-64.

[18] Sancho P, Barneda D, and Heeschen C. Hallmarks of cancer stem cell metabolism. Br J Cancer 2016.

[19] Luo M, and Wicha MS. Metabolic plasticity of cancer stem cells. Oncotarget 2015; 6: 35141-2.

[20] Dong C, Yuan T, Wu Y, Wang Y, Fan TW, Miriyala S, et al. Loss of FBP1 by Snail-mediated repression provides metabolic advantages in basal-like breast cancer. Cancer Cell 2013; 23: 316-31.

[21] Shen YA, Wang CY, Hsieh YT, Chen YJ, and Wei YH. Metabolic reprogramming orchestrates cancer stem cell properties in nasopharyngeal carcinoma. Cell Cycle 2015; 14: 86-98.

[22] D'Alessandro A, Amelio I, Berkers CR, Antonov A, Vousden KH, Melino G, et al. Metabolic effect of TAp63alpha: enhanced glycolysis and pentose phosphate pathway, resulting in increased antioxidant defense. Oncotarget 2014; 5: 7722-33.

[23] Gevi F, D'Alessandro A, Rinalducci S, and Zolla L. Alterations of red blood cell metabolome during cold liquid storage of erythrocyte concentrates in CPD-SAGM. J Proteomics 2012; 76 Spec No.: 168-80.

[24] Schulze A, and Harris AL. How cancer metabolism is tuned for proliferation and vulnerable to disruption. Nature 2012; 491: 364-73.
[25] Son J, Lyssiotis CA, Ying H, Wang X, Hua S, Ligorio M, et al. Glutamine supports pancreatic cancer growth through a KRAS-regulated metabolic pathway. Nature 2013; 496: 101-5.
[26] Moore PS, Sipos B, Orlandini S, Sorio C, Real FX, Lemoine NR, et al. Genetic profile of 22 pancreatic carcinoma cell lines. Analysis of K-ras, p53, p16 and DPC4/Smad4. Virchows Arch 2001; 439: 798-802.
[27] Fan J, Ye J, Kamphorst JJ, Shlomi T, Thompson CB, and Rabinowitz JD. Quantitative flux analysis reveals folate-dependent NADPH production. Nature 2014; 510: 298-302.
[28] Chen Q, Jin M, Zhu J, Xiao Q, and Zhang L. Functions of heterogeneous nuclear ribonucleoproteins in stem cell potency and differentiation. Biomed Res Int 2013; 2013: 623978.
[29] Hassa PO. The molecular "Jekyll and Hyde" duality of PARP1 in cell death and cell survival. Front Biosci (Landmark Ed) 2009; 14: 72-111.
[30] Lee JH, Han YS, and Lee SH. Long-Duration Three-Dimensional Spheroid Culture Promotes Angiogenic Activities of Adipose-Derived Mesenchymal Stem Cells. Biomol Ther (Seoul) 2016; 24: 260-7.
[31] Kim H. DNA repair Ku proteins in gastric cancer cells and pancreatic acinar cells. Amino Acids 2008; 34: 195-202.
[32] Puebla-Osorio N, Kim J, Ojeda S, Zhang H, Tavana O, Li S, et al. A novel Ku70 function in colorectal homeostasis separate from nonhomologous end joining. Oncogene 2014; 33: 2748-57.
[33] Jiang L, Wang H, Li J, Fang X, Pan H, Yuan X, et al. Up-regulated FASN expression promotes transcoelomic metastasis of ovarian cancer cell through epithelial-mesenchymal transition. Int J Mol Sci 2014; 15: 11539-54.
[34] Li J, Dong L, Wei D, Wang X, Zhang S, and Li H. Fatty acid synthase mediates the epithelial-mesenchymal transition of breast cancer cells. Int J Biol Sci 2014; 10: 171-80.
[35] Zaytseva YY, Rychahou PG, Gulhati P, Elliott VA, Mustain WC, O'Connor K, et al. Inhibition of fatty acid synthase attenuates CD44-associated signaling and reduces metastasis in colorectal cancer. Cancer Res 2012; 72: 1504-17.
[36] Mullen GE, and Yet L. Progress in the development of fatty acid synthase inhibitors as anticancer targets. Bioorg Med Chem Lett 2015; 25: 4363-9.
[37] Jiang P, Mukthavaram R, Chao Y, Nomura N, Bharati IS, Fogal V, et al. In vitro and in vivo anticancer effects of mevalonate pathway modulation on human cancer cells. Br J Cancer 2014; 111: 1562-71.
[38] Warita K, Warita T, Beckwitt CH, Schurdak ME, Vazquez A, Wells A, et al. Statin-induced mevalonate pathway inhibition attenuates the growth of mesenchymal-like cancer cells that lack functional E-cadherin mediated cell cohesion. Sci Rep 2014; 4: 7593.

Acknowledgments

This work was supported by AIRC 5 per mille grant n. 12182, Italy, the NIHR Liverpool Pancreas Biomedical Research Unit, and the Consorzio Interuniversitario Biotecnologie (CIB), Italy. I. Dando is a fellow of Fondazione Umberto Veronesi, Italy. E. Dalla Pozza is a fellow of ARC-Net (Applied Research on Cancer Network), University of Verona, Italy.

Competing financial interests: The authors declare no competing financial interests.

Figure Legends

Figure 1

Protein network of up-regulated proteins of Panc1 CSCs.

Schematic view of known and predicted protein interactions according to the STRING database (v. 10). Each node represents a protein, and each edge represents an interaction. Only interactions with the highest confidence score (0.700) are shown. Interactions include physical and functional associations, showing the evidence view. Thicker edges represent stronger associations.

Figure 2

Protein network of down-regulated proteins of Panc1 CSCs.

Schematic view of known and predicted protein interactions according to the STRING database (v. 10). Each node represents a protein, and each edge represents an interaction. Only interactions with the highest confidence score (0.700) are shown. Interactions include physical and functional associations, showing the evidence view. Thicker edges represent stronger associations.

Figure 3

IPA Canonical Pathways analysis.

The top 10 significantly altered canonical pathways associated with up-regulated (upper panel) and down-regulated (lower panel) proteins of Panc1 CSCs. The y-axis indicates the statistical significance calculated using the right-tailed Fisher exact test and the p value indicates the probability of association of proteins with the canonical pathway by random chance alone. Thus, taller bars equate to increased significance. The threshold line represents the default significance cut-off at $p = 0.05$. The ratio is calculated as follows: the number of molecules found in a given pathway divided by total number of molecules that constitute that specific canonical pathway.

683 The orange and blue coloured bars indicate predicted pathway activation, or predicted inhibition,
684 respectively (z-score). White bars are those with a z-score at or very close to 0. Grey bars indicate
685 pathways where no prediction can currently be made.
686
687 **Figure 4**
688 Western Blotting validation.
689 Differential expression of Panc1 CSC up-regulated (A) and down-regulated (B) proteins was verified
690 in two biological replicates (1 and 2). Proteins were resolved in 10-20% SDS-PAGE gels, transferred
691 onto PVDF membranes, and probed with specific antibodies against the indicated targets. Amido
692 Black staining was used as total loading control.
693
694 **Figure 5**
695 Metabolites analysis.
696 Absolute metabolomics quantification (arbitrary ion counts) of metabolites from glycolysis (A)
697 Pentose phosphate pathway (B) and Krebs cycle (C) in Panc1 parental cells (P; white histogram) and
698 Panc1 CSCs (black histogram). Values are presented as mean ± SD. The data were analyzed using
699 Student's t-test: * P< 0.05, ** P<0.01, and *** P<0.001 in Panc1 CSCs *versus* Panc1 P cells.
700
701 **Figure 6**
702 Anticancer effects of fatty acid and mevalonate pathways inhibition.
703 Cerulenin and atorvastatin effectively inhibited Panc1 CSCs viability. (A) Comparison of cerulenin
704 effects on Panc1 and Panc1 CSC cells viability. Cells were treated for 48 hours at doses ranging from
705 0 to 500 μM. (B) Evaluation of atorvastatin effects on Panc1 and Panc1 CSC cells viability. Cells were
706 treated for 48 hours at doses ranging from 0 to 250 μM. The data were analyzed using Student's t-test.
707 * P, 0.05.
708

Figure 7

Western Blotting analysis of Panc1 CSCs.

(A) FASN protein levels in Panc1 CSCs control (CTRL) and treated with cerulenin, and grown without EGF and FGF (- EGF/FGF). (B) ACAT2 protein levels in Panc1 CSCs control (CTRL) and treated atorvastatin. Proteins were resolved in 10-20% SDS-PAGE gels, transferred onto PVDF membranes, and probed with specific antibodies against the indicated targets. Amido Black staining was used as total loading control.

Figure 8

Cellular morphology after inhibition of fatty acid synthesis and mevalonate pathways.

Phase-contrast microscopy images of Panc1 and Panc1 CSCs after 24 hour of cerulenin (A) and atorvastatin (B) treatments.

Figure 9

Overview of key metabolic pathways in Panc1 CSCs. The up- and down-regulated proteins (enzymes) and metabolites identified in Panc1 CSCs compared to Panc1 P and mentioned into the discussion are shown in bold red and green, respectively. Proteins and metabolites that were not identified in this work are shown in gray. The inhibitors are shown in light blue.

729 **Table 1.** IPA-predicted top biological functions for up-regulated and down-regulated proteins of Panc1
730 CSCs.
731

Top Biological Functions (Panc1 CSCs up-regulated proteins)	P values[a] (ranging from)	No. of molecules[b]
Diseases and Disorders		
Dermatological Diseases and Conditions	1.21E-02 - 1.05E-10	34
Neurological Disease	1.21E-02 - 9.23E-09	49
Skeletal and Muscular Disorders	1.16E-02 - 9.23E-09	50
Psychological Disorders	1.21E-02 - 9.54E-09	34
Cancer	1.25E-02 - 3.13E-08	102
Molecular and Cellular Functions		
Cellular Growth and Proliferation	1.21E-02 - 1.17E-15	58
Cell Death and Survival	1.21E-02 - 1.80E-11	52
Cellular Development	1.21E-02 - 8.62E-08	34
Cellular Movement	1.24E-02 - 1.22E-06	30
Free Radical Scavenging	1.08E-02 - 1.50E-06	12
Physiological System Development and Function		
Cell-mediated Immune Response	1.21E-02 - 3.47E-05	4
Hematological System Development and Function	1.21E-02 - 3.47E-05	14
Immune Cell Trafficking	1.21E-02 - 3.47E-05	10
Endocrine System Development and Function	1.21E-02 - 5.40E-04	4
Organismal Survival	7.10E-04 - 7.10E-04	9

Top Biological Functions (Panc1 CSCs down-regulated proteins)	P values[a] (ranging from)	No. of molecules[b]
Diseases and Disorders		
Infectious Diseases	6.07E-03 - 2.85E-08	33
Dermatological Diseases and Conditions	6.07E-03 - 1.14E-07	22
Cancer	6.07E-03 - 2.15E-07	105
Organismal Injury and Abnormalities	6.07E-03 - 2.15E-07	105
Neurological Disease	6.07E-03 - 6.74E-07	42
Molecular and Cellular Functions		
Cellular Growth and Proliferation	6.07E-03 - 1.56E-18	64
RNA Post-Transcriptional Modification	6.07E-03 - 2.22E-17	23
Cell Death and Survival	6.07E-03 - 2.24E-15	54
Cellular Development	6.07E-03 - 8.12E-10	55
Cellular Response to Therapeutics	1.00E-03 - 1.48E-09	7
Physiological System Development and Function		
Skeletal and Muscular System Development and Function	1.09E-04 - 8.12E-10	12
Tissue Development	6.07E-03 - 8.12E-10	30
Cardiovascular System Development and Function	6.07E-03 - 3.70E-07	18
Organismal Development	6.07E-03 - 3.70E-07	21
Hair and Skin Development and Function	6.07E-03 - 2.03E-05	11

732
733 [a] Fisher's exact test was used to calculate a p value for each protein of the dataset identified in the biological function studied, indicating the probability
734 that each biological function assigned to the data set is assigned by chance; then we have a range of p values corresponding to all p values calculated for
735 all proteins of the dataset in the biological function. [b] The number of molecules of the differentially expressed protein dataset is shown.
736

737

738

Figure 1

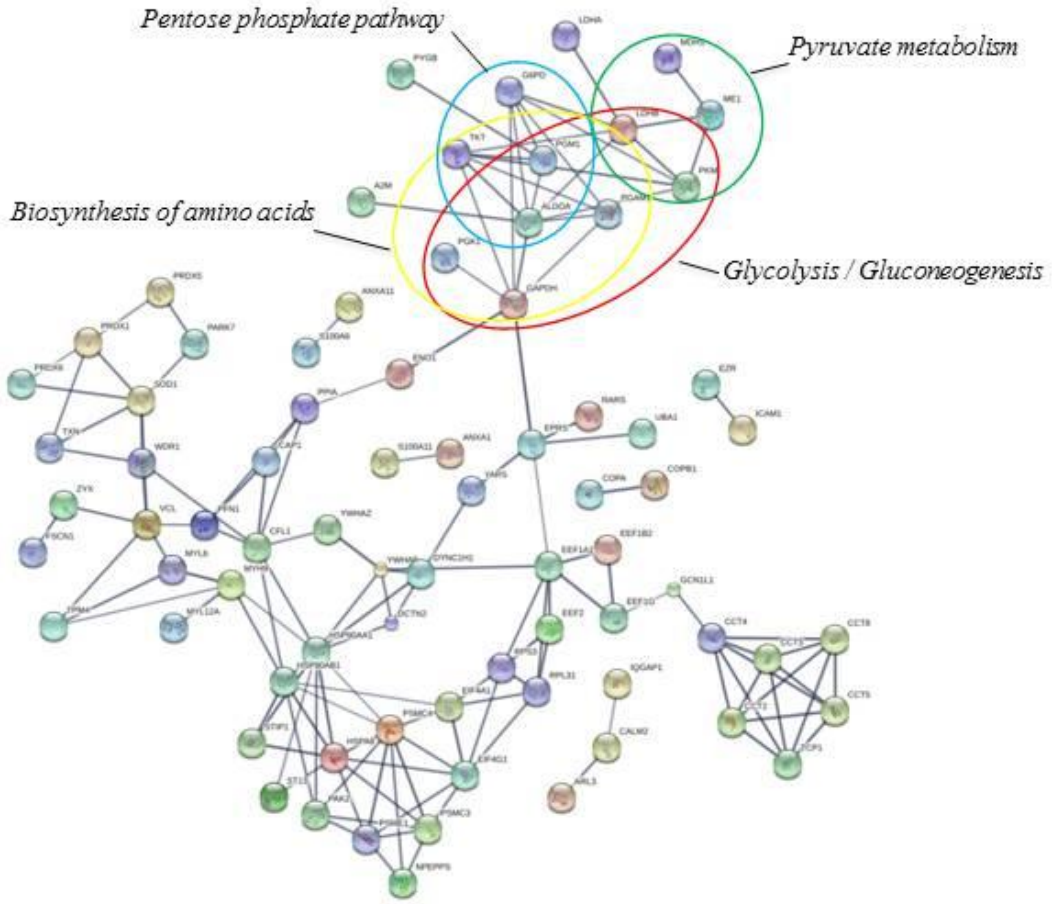
Pentose phosphate pathway
Pyruvate metabolism
Biosynthesis of amino acids
Glycolysis / Gluconeogenesis

752 **Figure 2**

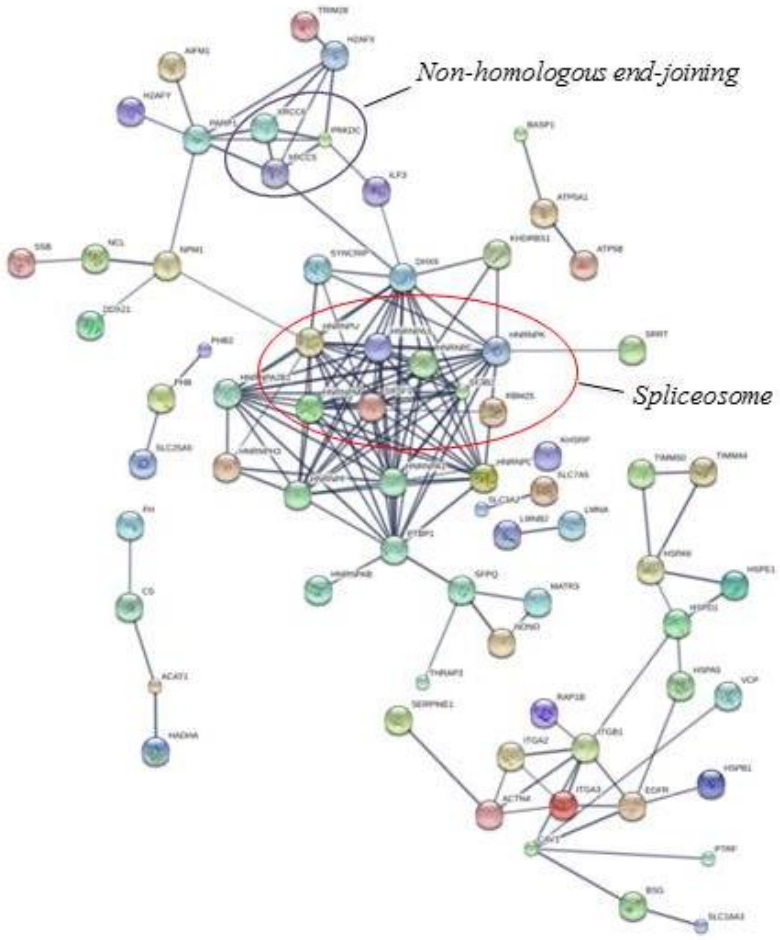

753

754

Figure 3

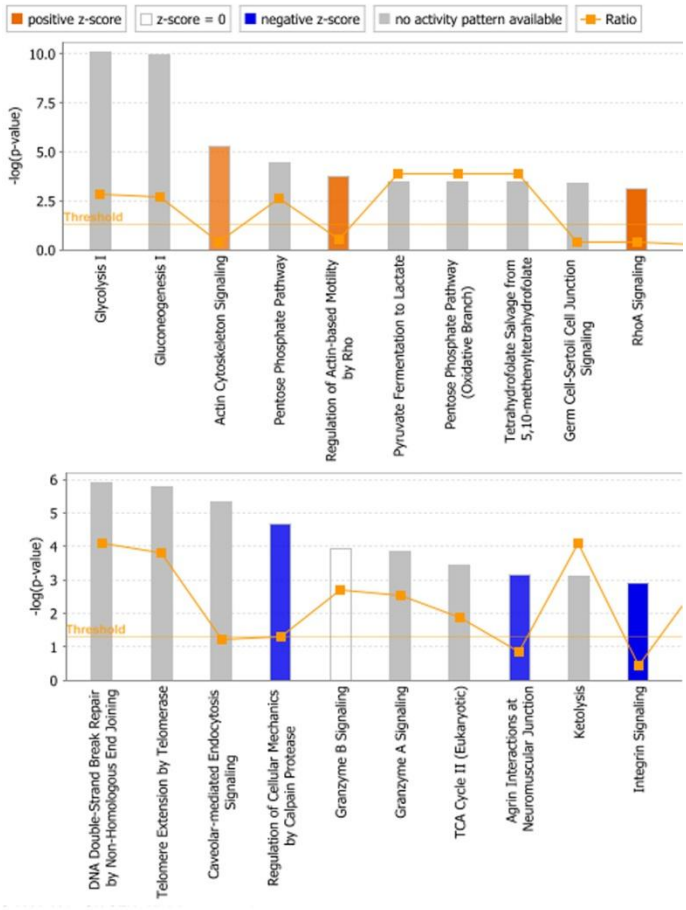
positive z-score
z-score = 0
negative z-score
no activity pattern available
Ratio
-log(p-value)
10.0
7.5
5.0
2.5
0.0
Threshold
Glycolysis I
Gluconeogenesis I
Actin Cytoskeleton Signaling
Pentose Phosphate Pathway
Regulation of Actin-based Motility by Rho
Pyruvate Fermentation to Lactate
Pentose Phosphate Pathway (Oxidative Branch)
Tetrahydrofolate Salvage from 5,10-methenyltetrahydrofolate
Germ Cell-Sertoli Cell Junction Signaling
RhoA Signaling
-log(p-value)
6
5
4
3
2
1
0
Threshold
DNA Double-Strand Break Repair by Non-Homologous End Joining
Telomere Extension by Telomerase
Caveolar-mediated Endocytosis Signaling
Regulation of Cellular Mechanics by Calpain Protease
Granzyme B Signaling
Granzyme A Signaling
TCA Cycle II (Eukaryotic)
Agrin Interactions at Neuromuscular Junction
Ketolysis
Integrin Signaling

Figure 4

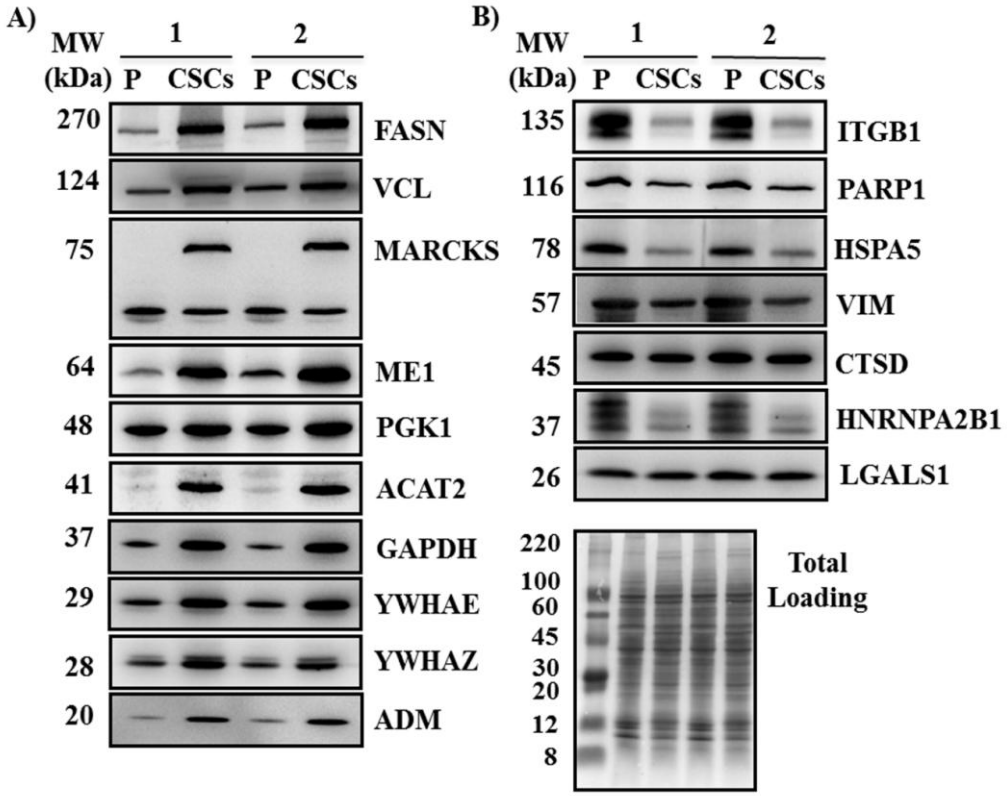
A)
MW (kDa)
1
2
P
CSCs
P
CSCs
270
FASN
124
VCL
75
MARCKS
64
ME1
48
PGK1
41
ACAT2
37
GAPDH
29
YWHAE
28
YWHAZ
20
ADM
B)
MW (kDa)
1
2
P
CSCs
P
CSCs
135
ITGB1
116
PARP1
78
HSPA5
57
VIM
45
CTSD
37
HNRNPA2B1
26
LGALS1
220
100
60
45
30
20
12
8
Total Loading

Figure 5

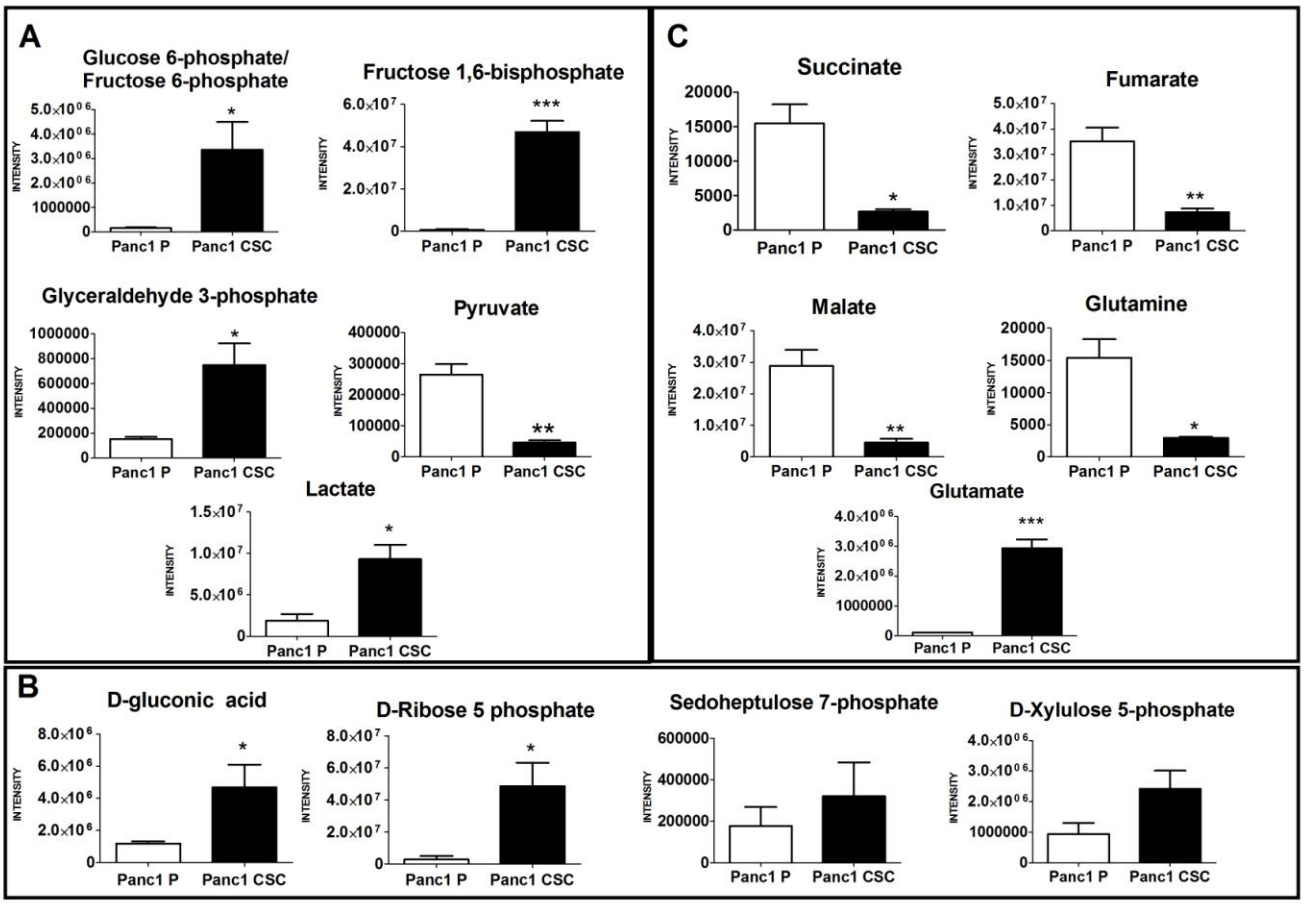
A
Glucose 6-phosphate/ Fructose 6-phosphate
Fructose 1,6-bisphosphate
Glyceraldehyde 3-phosphate
Pyruvate
Lactate
C
Succinate
Fumarate
Malate
Glutamine
Glutamate
B
D-gluconic acid
D-Ribose 5 phosphate
Sedoheptulose 7-phosphate
D-Xylulose 5-phosphate
INTENSITY
Panc1 P
Panc1 CSC

778 **Figure 6**

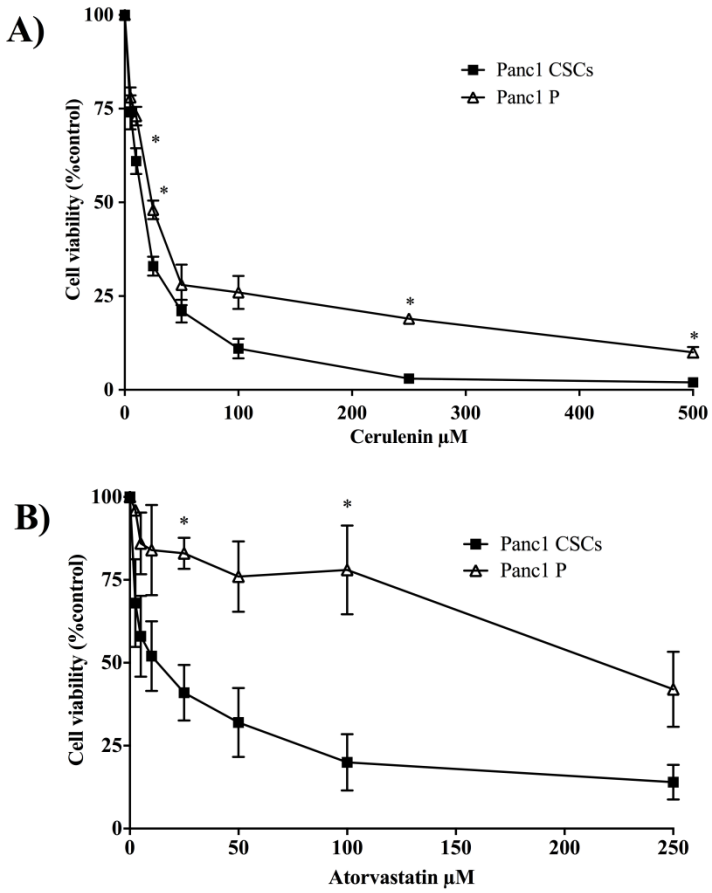

779

780

781

782

783 **Figure 7**

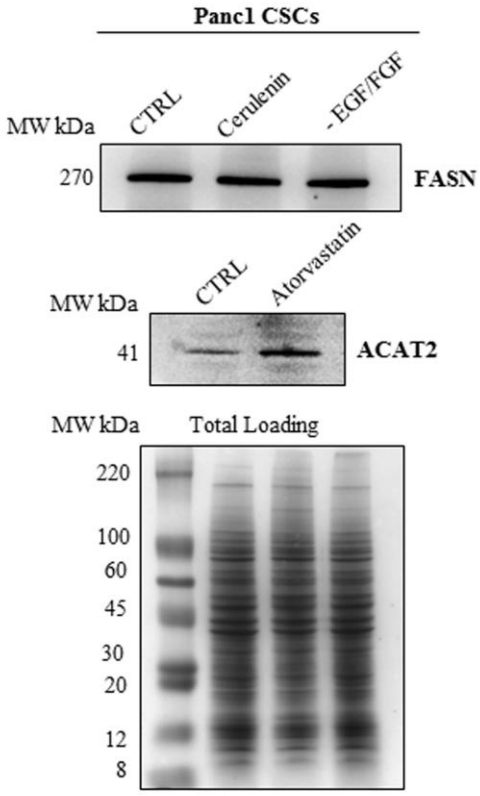

784

785 **Figure 8**

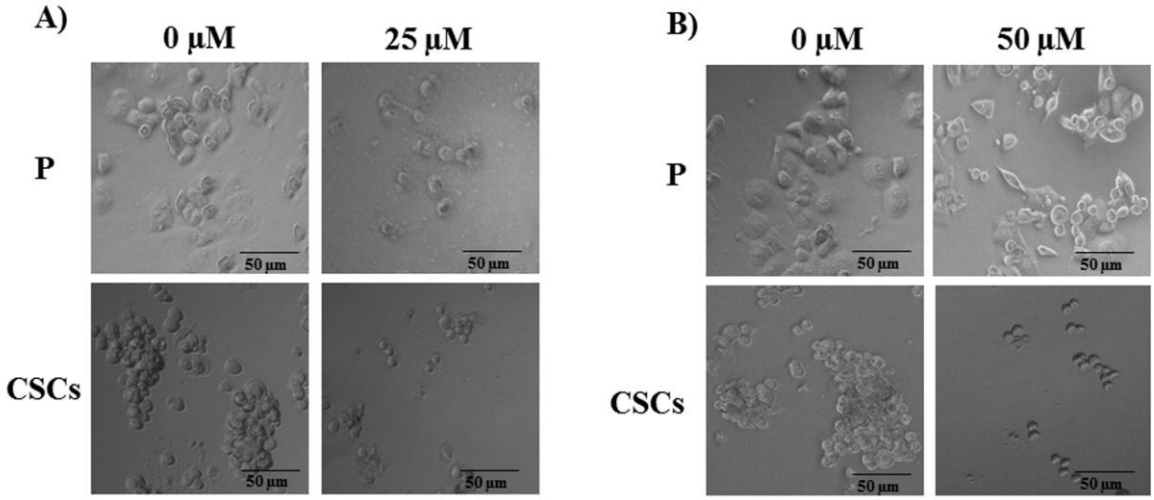

786

Figure 9

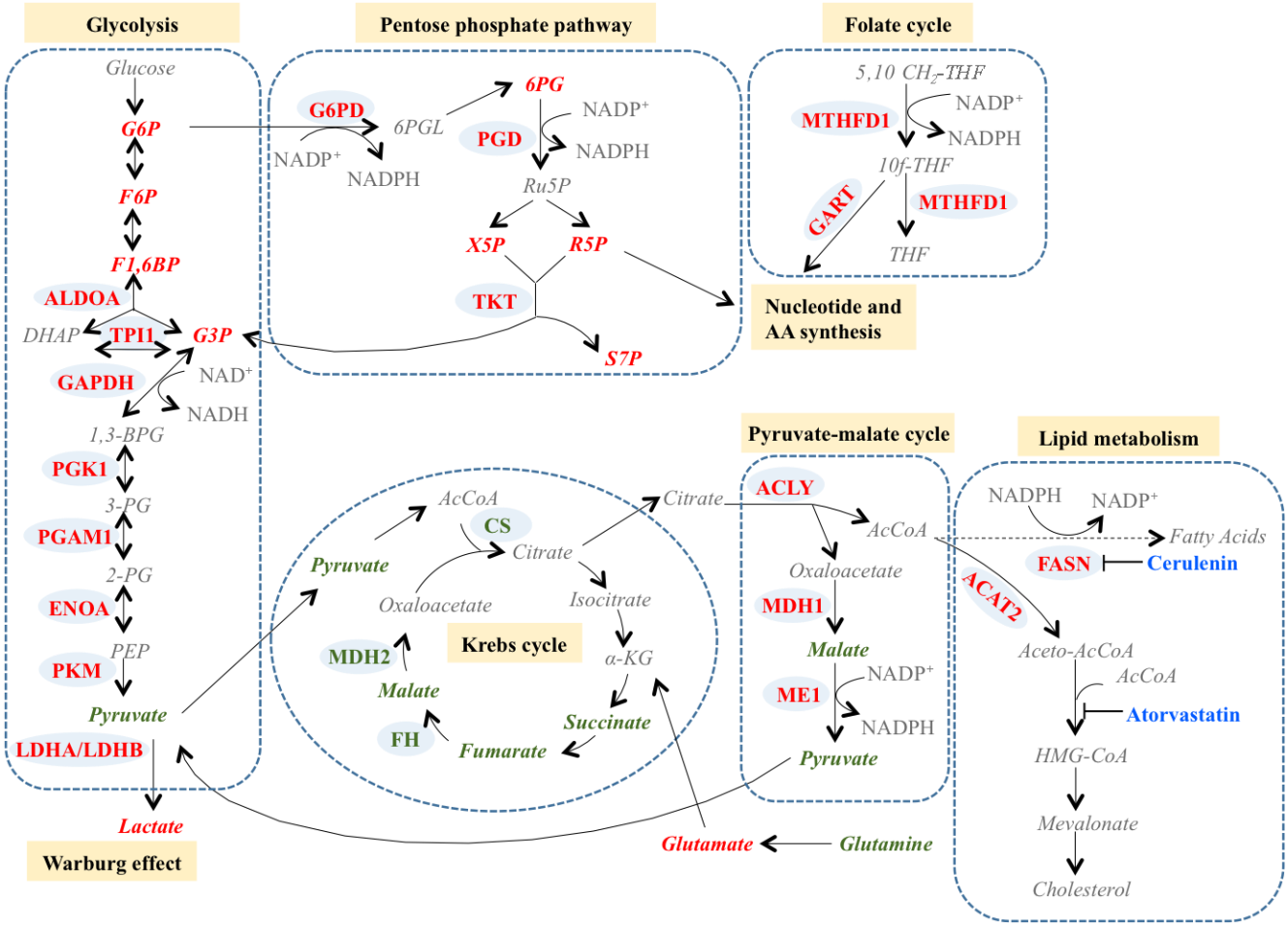
Glycolysis
Pentose phosphate pathway
Folate cycle
Glucose
G6P
F6P
F1,6BP
ALDOA
DHAP
TPI1
G3P
GAPDH
NAD+
NADH
1,3-BPG
PGK1
3-PG
PGAM1
2-PG
ENOA
PEP
PKM
Pyruvate
LDHA/LDHB
Lactate
Warburg effect
G6PD
6PGL
NADP+
NADPH
6PG
PGD
Ru5P
X5P
R5P
TKT
S7P
5,10 CH2-THF
MTHFD1
10f-THF
GART
THF
Nucleotide and AA synthesis
AcCoA
CS
Citrate
Pyruvate
Oxaloacetate
Isocitrate
MDH2
Krebs cycle
α-KG
Malate
Succinate
FH
Fumarate
Pyruvate-malate cycle
ACLY
AcCoA
Oxaloacetate
MDH1
Malate
ME1
NADP+
NADPH
Pyruvate
Glutamate
Glutamine
Lipid metabolism
NADPH
NADP+
Fatty Acids
FASN
Cerulenin
ACAT2
Aceto-AcCoA
AcCoA
Atorvastatin
HMG-CoA
Mevalonate
Cholesterol

supplemental Figure 1 (networks alterations)

Click here to download Supplementary material: supplemental Figure 1 (networks alterations).doc

supplemental Table 1 (antibodies used for western blotting valid

Click here to download Supplementary material: supplemental Table 1 (antibodies used for western blotting validation).doc

Supplemental Table 2 (2045 identified proteins, 1157 quantified

Click here to download Supplementary material: Supplemental Table 2 (2045 identified proteins, 1157 quantified proteins).xls

Supplemental Table 3 (n=608 identification via single peptide)

Click here to download Supplementary material: Supplemental Table 3 (n=608 identification via single peptide).xls

Supplemental Table 4 (n=230 differentially expressed)

Click here to download Supplementary material: Supplemental Table 4 (n=230 differentially expressed).xlsx

Supplemental Table 5 (Canonical pathways enriched)

Click here to download Supplementary material: Supplemental Table 5 (Canonical pathways enriched).xlsx

Supplemental Table 6 (upstream regulators)

Click here to download Supplementary material: Supplemental Table 6 (upstream regulators).xlsx

***Conflict of Interest**

Click here to download Conflict of Interest: Conflict of interest.docx